Microscopic theory of the collective atomic recoil laser in an optical resonator: The effects of collisions

Mathias Perrin,[1] Zongxiong Ye,[2] and Lorenzo M. Narducci[2]
[1]*INLN, 1361 Route des Lucioles, Sophia Antipolis, 06560 Valbonne, France*
[2]*Department of Physics, Drexel University, Philadelphia, Pennsylvania 19104*
(Received 8 July 2002; published 22 October 2002)

With the help of a microscopic model we investigate the effects of collisions and atomic recoil on the behavior of absorbing atoms placed inside a bidirectional resonator and driven by an external injected field. This model complements and generalizes earlier studies of the collective atomic recoil laser and of optical bistability. According to our model, even in the presence of collisions, the resonator can support bidirectional propagation. In particular, for appropriate selection of the parameters, we predict the existence of stationary solutions such that the cavity field that copropagates with the injected signal is locked in frequency with the external source, while the counterpropagating field is frequency shifted from both, even in steady state. The early stage of growth of the counterpropagating field is accompanied by a spatial modulation (grating structure) in the density of the medium, but this modulation decays away in a time roughly of the order of the average interval between collisions.

DOI: 10.1103/PhysRevA.66.043809 PACS number(s): 42.55.Ah, 42.50.Vk, 42.65.Pc, 42.65.Sf

I. INTRODUCTION

In a recent paper [1] two of us developed a description of a driven bidirectional ring resonator containing a collection of two-level absorbing atoms. The objective of that work was to generalize the well established plane-wave model of optical bistability [2] by taking into account the possible growth of a cavity field in a direction opposite to that of the injected signal.

An important step along this line had already been taken by Asquini and Casagrande [3] under resonance conditions, a setting where the frequency of the driving field matches one of the cavity modes and the atomic transition frequency. By relaxing the resonance requirement, and for appropriate values of the system parameters, we discovered in [1] that the ring resonator can support simultaneously both a forward and a backward field in steady state [4]. This stationary solution may in turn become unstable and give way to self-pulsing and other instabilities.

A surprising feature of the stationary solutions is that, while the forward field is locked to the frequency of the injected signal, as one would expect, the backward field oscillates, instead, at a different frequency. With the help of numerical calculations we found that this frequency is typically comparable to what one can estimate on the basis of the usual mode-pulling formula of ordinary laser theory. At first sight, this is surprising on two accounts: one would not expect that a resonator could support a stationary state in which two fields have different carrier frequencies and, furthermore, the medium in the cavity is not active in the conventional sense, i.e., prepared in a state of population inversion.

We interpreted this behavior by attributing the initial growth of the backward field to spontaneous emission noise in the presence of a gain feature impressed upon the atomic absorption profile by the forward field, perhaps something akin to the gain that emerges when a passive two-level atom is driven by a strong field. When the backward gain is sufficiently large to overcome the cavity losses, we argued that the backward field can grow and eventually reach a steady state, much as an ordinary laser field would in a ring cavity. According to this interpretation, the frequency shift of the backward field would then be the consequence of the usual competition between oscillations at the peak of the atomic gain feature and at the frequency of the nearest cavity mode (i.e., mode pulling).

The growth mechanism of the backward field is reminiscent of the physics of a different system, the collective atomic recoil laser (CARL) [5]. In its original conception and according to the simplest version of the model, the CARL system consists of a collection of two-level atoms driven by a single-mode pump field. Under appropriate conditions, atomic density fluctuations, together with population and polarization fluctuations, induce a small amount of backscattering which interferes with the pump field and creates a weak traveling modulation wave. This, in turn, generates a weak reverse polarization wave which, for appropriate values of the parameters, radiates and strengthens the backward scattered field in an avalanche process. An essential feature of the CARL model is the dynamical role played by the atomic center of mass degrees of freedom. These must be included in the theoretical description to give proper account of recoil effects, which eventually are responsible for producing an organized atomic density modulation, or density grating, which is at the heart of the CARL process (hence the terms ''collective atomic recoil'' in the descriptor). Attempts to demonstrate the CARL action experimentally [6] have led to the identification of a strong backward field with some of the expected characteristics. However, it is fair to say that a clear link between the observed backward field and the expected density grating has not yet been established, as argued, convincingly in our opinion, in further theoretical and experimental contributions by Gauthier and collaborators [7].

In this paper we generalize the bidirectional ring cavity model of Ref. [1] to include consideration of the atomic center of mass degrees of freedom, with the eventual aim of

formulating the theory of the CARL in a resonator from first principles, with full account of the cavity geometry and boundary conditions [8]. This generalization, simple enough in principle, is confronted at once with a basic difficulty. The CARL equations developed in [5] include the well known phenomenological relaxation terms for the atomic population and polarization variables, which are essential for the establishment of a steady state in ordinary laser theories. However, they do not include a mechanism by which the atomic center of mass momenta can approach a thermal equilibrium state if the cavity field should be turned off. This difficulty of the CARL model was made clear by the earliest numerical simulations [5] which never gave any indication that the system would approach a steady state for long times. Thus, the appearance of a backward pulse of light could be traced to the initial creation of a density grating, as evidenced by the large values taken by the bunching parameter, but the subsequent evolution of the system was highly irregular, and its physical significance questionable in the absence of a thermalization mechanism for the atomic momenta. An appealing attempt to resolve this problem was made in Ref. [9] with the inclusion of a phenomenological relaxation term in the momentum equation. In this work we have made an attempt to compare our findings with those of Ref. [9]. We discuss our available results, but we feel that they are not sufficient to reach an informed conclusion. Further studies would be desirable for the purpose of confirming the reliability of the phenomenological approach.

An alternative solution to this problem was advanced in Ref. [10] where the authors generalized the two-mode model of the CARL [5] with explicit consideration of the collisions undergone by the optically active atoms with a buffer gas at thermal equilibrium. The collisions were included following a procedure inspired by molecular dynamical simulations. This is an important improvement over the traditional CARL model not only on theoretical grounds, but also because a buffer gas was actually used in some of the experiments, and indeed it played a crucial role for the purpose of establishing an eventual steady state, as shown in [10].

Following this lead, our present generalization of the driven bidirectional ring cavity model [1] includes the center of mass degrees of freedom among the dynamical variables, and it also simulates the collisional interactions between the atoms and the buffer gas. Collisions among the optically active atoms are, instead, ignored, under the assumption that these are far more rare in a typical experimental setting, where the density of these atoms is several orders of magnitude smaller than that of the buffer gas.

Our numerical investigations of this model have shown that, even in the presence of collisions and for appropriate values of the parameters, the resonator can support the growth of a backward field. Forward and backward fields may approach a stationary state for sufficiently long times or self-pulsing states, although sometimes only the forward field survives in a pulsing mode.

These features are qualitatively similar to those reported in [1]. However, the microscopic nature of our model allows us to raise more detailed questions than could be addressed in our earlier contribution. Thus, we have explored the possible emergence of a density grating, or a spatial modulation of the atomic density, which is usually regarded as the main signature of the CARL process. We found that, during the early phase of growth of the backward field, a grating structure indeed appears, but that it then decays in a time of the order of the average interval between collisions.

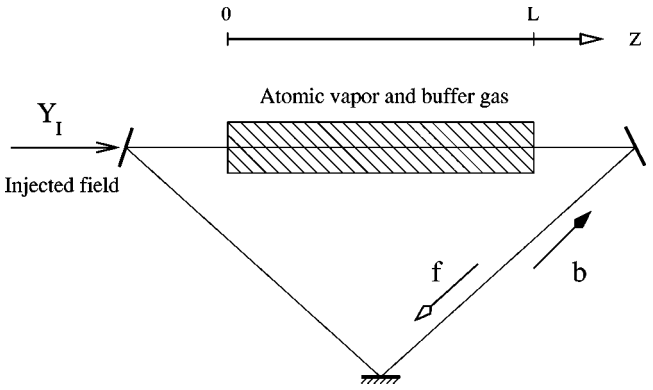

FIG. 1. Schematic representation of the bidirectional ring cavity; *f* and *b* denote the forward and backward cavity fields, respectively, and Y_I is the scaled amplitude of the injected field.

We have also explored the momentum distribution of the atoms under the driving action of the cavity fields (and the collisions), and tried to correlate our findings with simulations based on the proposal of Ref. [9]. As already mentioned, we have had only limited success in assessing the possible connection between these approaches: for some parameter values we found acceptable qualitative agreement between the dynamical evolution of the cavity fields while, for others, the solutions differed drastically (time-independent versus self-pulsing behavior, for example). Surprisingly, when the long time momentum distributions predicted by the two procedures agreed well with each other, the respective field evolutions showed little or no resemblance, and vice versa. Nevertheless, we have tried to come up with a possible interpretation for the appearance of these features.

The paper is organized as follows. In Sec. II we outline the derivation of the deterministic equations forming the backbone of the numerical simulations. Section III contains a general outline of the approach for handling the collisions of the optically active atoms with the buffer gas. In Sec. IV we summarize the most relevant results of our simulations including a comparison between our approach and the one introduced in Ref. [9]. We complete the paper with some concluding remarks and an Appendix where we summarize qualitatively the essential steps of the collisional simulation.

II. DERIVATION OF THE EQUATIONS OF MOTION

Our goal is to study the behavior of a collection of two-level absorbing atoms placed within a ring resonator and driven by an external coherent field as shown schematically in Fig. 1. In general, one expects the cavity field to propagate both in the forward and in the backward directions. Our approach draws from techniques developed in Refs. [1] and [5] but it also departs from these previous works in several significant aspects. Thus, as in Ref. [1], we are especially inter-

ested in the growth and characterization of the backward field, and this requires appropriate modifications of the resonator boundary conditions relative to the traditional setting of optical bistability. However, unlike these older studies, our present investigations include the center of mass motion of the optically active atoms. As it turns out, this precludes the use of the collective population and polarization variables which are very convenient and quite common in ordinary laser theory. The price one has to pay for this generalization is that each atom must be described by its own set of dynamical variables, including the center of mass position and momentum.

This latter feature is common to the CARL theory [5], which, as originally designed, does not describe from first principles the role of the resonator, its role in creating a feedback mechanism, and the effects of possible detunings. In addition, as already mentioned, the emergence of an eventual steady state requires the existence of a process by which the optically active atoms can reach thermal equilibrium, and such a mechanism is also absent from the original CARL model.

A feature common to the theory of the CARL and the present work is the adoption of the semiclassical approximation and the replacement of the atomic operators with corresponding ordinary *c*-number functions. In view of these similarities and differences, and for the purpose of making this work reasonably self-contained, we begin with a detailed description of the model and a derivation of the relevant equations of motion.

Our starting point is provided by the Hamiltonian

$$H=\hbar\omega_A\sum_{j=1}^{N}S_{zj}+\sum_{j=1}^{N}\frac{p_j^2}{2m}-\sum_{j=1}^{N}\mu(S_j^+ + S_j^-)\mathcal{E}(z_j,t), \quad (1)$$

where the population difference operator for the jth atom, S_{zj}, and the polarization operator S_j^+ are defined by

$$S_{zj}=\frac{1}{2}\begin{pmatrix}1 & 0\\ 0 & -1\end{pmatrix}, \quad S_j^+=\begin{pmatrix}0 & 1\\ 0 & 0\end{pmatrix}, \quad (2)$$

and $S_j^-=(S_j^+)^\dagger$. The operators p_j and z_j are the canonically conjugate momentum and position of the jth atom, μ is the modulus of the transition dipole moment, and $\mathcal{E}(z_j,t)$ is the classical cavity field at the location of the jth atom.

The atomic Heisenberg equations, after carrying out the semiclassical approximation, are

$$\frac{d}{dt}z_j=\frac{p_j}{m}, \quad (3a)$$

$$\frac{d}{dt}p_j=\mu(S_j^+ + S_j^-)\frac{\partial}{\partial z_j}\mathcal{E}(z_j,t), \quad (3b)$$

$$\frac{d}{dt}S_j^-=-i\omega_A S_j^- - 2i\frac{\mu}{\hbar}\mathcal{E}(z_j,t)S_{zj}, \quad (3c)$$

$$\frac{d}{dt}S_{zj}=i\frac{\mu}{\hbar}\mathcal{E}(z_j,t)(S_j^+ - S_j^-). \quad (3d)$$

The cavity field obeys the wave equation

$$\frac{\partial^2\mathcal{E}(z,t)}{\partial t^2}-c^2\frac{\partial^2\mathcal{E}(z,t)}{\partial z^2}=-\frac{1}{\epsilon_0}\frac{\partial^2\mathcal{P}(z,t)}{\partial t^2}, \quad (4)$$

where $\mathcal{P}(z,t)$ is the macroscopic dipole moment per unit volume. We assume the cavity field to have the form

$$\mathcal{E}(z,t)=\mathcal{E}_F(z,t)+\mathcal{E}_B(z,t), \quad (5)$$

where

$$\mathcal{E}_F(z,t)=E_F(z,t)e^{i(kz-\omega t)}+\text{c.c.}, \quad (6a)$$

$$\mathcal{E}_B(z,t)=E_B(z,t)e^{-i(kz+\omega t)}+\text{c.c.}, \quad (6b)$$

and F and B label the forward and the backward directions of propagation, respectively. The injected field is given by

$$\mathcal{E}_I(z,t)=E_I e^{i(kz-\omega t)}+\text{c.c.}, \quad (7)$$

where E_I is a real constant amplitude. Its carrier frequency ω and wave number $k=\omega/c$ are selected as the reference frequency and wave number, respectively.

In light of the near resonant interaction between the injected field and the atoms, the amplitudes $E_F(z,t)$ and $E_B(z,t)$ are slowly varying with respect to both z and t. Thus, the cavity field $\mathcal{E}(z,t)$ is a superposition of two contributions that propagate in opposite directions with slowly varying amplitudes.

For the macroscopic polarization that appears on the right hand side of Eq. (4) we assume the representation

$$\mathcal{P}(z,t)=\mu[P^{(+)}(z,t)e^{-i\omega t}+P^{(-)}(z,t)e^{i\omega t}], \quad (8)$$

where $P^{(\pm)}(z,t)$ are slowly varying functions of time, but rapidly varying functions of space. Moreover, we have $P^{(-)}(z,t)=[P^{(+)}(z,t)]^*$.

Following the procedure adopted in Refs. [11] and [1], the field equations for the slowly varying amplitudes are

$$\left(\frac{\partial}{\partial t}+c\frac{\partial}{\partial z}\right)E_F(z,t)=i\frac{\omega\mu}{2\epsilon_0}\frac{1}{\lambda}\int_z^{z+\lambda}dz' e^{-ikz'}P^{(+)}(z',t), \quad (9a)$$

$$\left(\frac{\partial}{\partial t}-c\frac{\partial}{\partial z}\right)E_B(z,t)=i\frac{\omega\mu}{2\epsilon_0}\frac{1}{\lambda}\int_z^{z+\lambda}dz' e^{ikz'}P^{(+)}(z',t). \quad (9b)$$

The cavity field is further constrained by the boundary conditions which, for the empty resonator, have the form

$$\mathcal{E}_F(0,t)=\sqrt{T}\mathcal{E}_I(0,t)+R\mathcal{E}_F(\Lambda,t), \quad (10a)$$

$$\mathcal{E}_B(\Lambda,t)=R\mathcal{E}_B(0,t), \quad (10b)$$

where Λ is the round-trip length of the ring cavity, and R and T are, respectively, the power reflection and transmission coefficients. In terms of the slowly varying amplitudes, Eqs. (10) become

$$E_F(0,t)=\sqrt{T}E_I+RE_F(\Lambda,t)e^{-i\delta}, \tag{11a}$$

$$E_B(\Lambda,t)=RE_B(0,t)e^{-i\delta}, \tag{11b}$$

where $\delta=(\omega_C-\omega)\Lambda/c$, and ω_C is one of the cavity resonances. Specifically, we select ω_C as the frequency of the cavity mode that is nearest to the atomic transition frequency.

The atomic equations (3) and the field equations (9) are coupled to each other by virtue of the following link between the macroscopic polarization and the microscopic internal variables $S_j^{\pm}$:

$$\mathcal{P}(z,t)=\frac{\mu}{A}\sum_{j=1}^{N}\delta(z-z_j(t))(S_j^{+}+S_j^{-}), \tag{12}$$

where A is the cross sectional area of the atomic sample. Upon introducing the slowly varying variables $\tilde{S}_j$ and $\tilde{S}_j^*$ according to the relations

$$S_j^{-}=\tilde{S}_j e^{-i\omega t}, \quad S_j^{+}=\tilde{S}_j^* e^{i\omega t}, \tag{13}$$

the macroscopic polarization takes the form given by Eq. (8) with

$$P^{(+)}(z,t)=\frac{1}{A}\sum_{j=1}^{N}\delta(z-z_j(t))\tilde{S}_j, \tag{14a}$$

$$P^{(-)}(z,t)=\frac{1}{A}\sum_{j=1}^{N}\delta(z-z_j(t))\tilde{S}_j^*. \tag{14b}$$

Finally, we only need to write the atomic and field equations in terms of $\tilde{S}_j$, E_F, and E_B and their complex conjugate variables, with the result

$$\frac{dz_j}{dt}=\frac{p_j}{m}, \tag{15a}$$

$$\frac{dp_j}{dt}=-ik\mu\tilde{S}_j[E_F^*(z_j,t)e^{-ikz_j}-E_B^*(z_j,t)e^{ikz_j}]+\text{c.c.}, \tag{15b}$$

$$\frac{d\tilde{S}_j}{dt}=i(\omega-\omega_A)\tilde{S}_j-2i\frac{\mu}{\hbar}S_{zj}[E_F(z_j,t)e^{ikz_j}+E_B(z_j,t)e^{-ikz_j}], \tag{15c}$$

$$\frac{dS_{zj}}{dt}=i\frac{\mu}{\hbar}\tilde{S}_j^*[E_F(z_j,t)e^{ikz_j}+E_B(z_j,t)e^{-ikz_j}]+\text{c.c.}, \tag{15d}$$

$$\left(\frac{\partial}{\partial t}+c\frac{\partial}{\partial z}\right)E_F=i\frac{\omega\mu}{2\epsilon_0}\frac{1}{A\lambda}\int_z^{z+\lambda}dz'e^{-ikz'}\times\sum_{j=1}^{N}\delta(z'-z_j)\tilde{S}_j, \tag{15e}$$

$$\left(\frac{\partial}{\partial t}-c\frac{\partial}{\partial z}\right)E_B=i\frac{\omega\mu}{2\epsilon_0}\frac{1}{A\lambda}\int_z^{z+\lambda}dz'e^{ikz'}\times\sum_{j=1}^{N}\delta(z'-z_j)\tilde{S}_j. \tag{15f}$$

These equations are to be solved with the additional constraints provided by the boundary conditions (11). Note that, in taking the spatial derivatives of the field on the right hand side of Eq. (3b), we have explicitly accounted for the slow spatial variation of the amplitudes E_F and E_B. Moreover, in arriving at Eqs. (15b), (15c), and (15d) we have omitted factors that vary rapidly in time at frequencies $\pm 2\omega$.

Scaled variables and the uniform field limit

Our next objective is to derive the final form of the equations in the so-called uniform-field limit [12]. For this purpose it would be especially convenient if the boundary conditions were of the standard periodicity type. This can be arranged by introducing a new set of cavity field amplitudes $Y_F(z,t)$ and $Y_B(z,t)$, and the injected field amplitude Y_I, which, in scaled dimensionless form, are defined by the relations

$$E_F(z,t)=\frac{\hbar}{2\mu}(\gamma_\parallel\gamma_\perp)^{1/2}\left(Y_F(z,t)-\frac{z}{\Lambda}|\ln R|Y_I\right)\times\exp\left[-\frac{z}{\Lambda}\ln(\mathrm{Re}^{-i\delta})\right], \tag{16a}$$

$$E_B(z,t)=\frac{\hbar}{2\mu}(\gamma_\parallel\gamma_\perp)^{1/2}Y_B(z,t)\exp\left[\frac{z-\Lambda}{\Lambda}\ln(\mathrm{Re}^{-i\delta})\right], \tag{16b}$$

$$E_I=\frac{\hbar}{2\mu}(\gamma_\parallel\gamma_\perp)^{1/2}\frac{|\ln R|}{\sqrt{T}}Y_I. \tag{16c}$$

It is a simple matter to verify that, indeed, in terms of the transformed field variables, the boundary conditions (11) take the form

$$Y_F(0,t)=Y_F(\Lambda,t), \tag{17a}$$

$$Y_B(\Lambda,t)=Y_B(0,t). \tag{17b}$$

It is also convenient to introduce the scaled atomic variables σ_j and σ_{zj} according to the definitions

$$\tilde{S}_j=-\frac{i}{2}\left(\frac{\gamma_\parallel}{\gamma_\perp}\right)^{1/2}\sigma_j, \quad S_{zj}=\frac{1}{2}\sigma_{zj}, \tag{18}$$

and the parameters

$$\alpha=\frac{\mathfrak{N}\omega\mu^2}{2\hbar\gamma_\perp\epsilon_0 c},\quad \kappa=\frac{c|\ln R|}{\Lambda},\tag{19}$$

where $\mathfrak{N}=N/(AL)$ is the number of atoms per unit volume and L is the length of the sample. We recognize α as the unsaturated field absorption coefficient per unit length, and κ as the damping rate of the field amplitude out of the cavity (or the linewidth of the cavity mode).

In terms of the new variables, the equations of motion take the form

$$\frac{dz_j}{dt}=\frac{p_j}{m},\tag{20a}$$

$$\frac{dp_j}{dt}=-\frac{\hbar k}{4}\gamma_\parallel\sigma_j\left(Y_F^*-\frac{z_j}{\Lambda}|\ln R|Y_I\right)\exp\left[-\frac{z_j}{\Lambda}\ln(Re^{i\delta})\right]e^{-ikz_j}+\frac{\hbar k}{4}\gamma_\parallel\sigma_j Y_B^*\exp\left[\frac{z_j-\Lambda}{\Lambda}\ln(Re^{i\delta})\right]e^{ikz_j}+\text{c.c.},\tag{20b}$$

$$\frac{d\sigma_j}{dt}=i(\omega-\omega_A)\sigma_j+\gamma_\perp\sigma_{zj}\left(Y_F-\frac{z_j}{\Lambda}|\ln R|Y_I\right)\exp\left[-\frac{z_j}{\Lambda}\ln(Re^{-i\delta})\right]e^{ikz_j}+\gamma_\perp\sigma_{zj}Y_B\exp\left[\frac{z_j-\Lambda}{\Lambda}\ln(Re^{-i\delta})\right]e^{-ikz_j},\tag{20c}$$

$$\frac{d\sigma_{zj}}{dt}=-\frac{\gamma_\parallel}{2}\sigma_j\left(Y_F^*-\frac{z_j}{\Lambda}|\ln R|Y_I\right)\exp\left[-\frac{z_j}{\Lambda}\ln(Re^{i\delta})\right]e^{-ikz_j}-\frac{\gamma_\parallel}{2}\sigma_j Y_B^*\exp\left[\frac{z_j-\Lambda}{\Lambda}\ln(Re^{i\delta})\right]e^{ikz_j}+\text{c.c.},\tag{20d}$$

$$\left(\frac{\partial}{\partial t}+c\frac{\partial}{\partial z}\right)Y_F=\kappa Y_I-\kappa\left(1+i\frac{\delta}{|\ln R|}\right)Y_F+\kappa^2\left(1+i\frac{\delta}{|\ln R|}\right)\frac{z}{c\Lambda}Y_I+\frac{cL\alpha}{\lambda N}\exp\left[\frac{z}{\Lambda}\ln(\mathrm{Re}^{-i\delta})\right]\int_z^{z+\lambda}dz'e^{-ikz'}\sum_{j=1}^{N}\delta(z'-z_j)\sigma_j,\tag{20e}$$

$$\left(\frac{\partial}{\partial t}-c\frac{\partial}{\partial z}\right)Y_B=-\kappa\left(1+i\frac{\delta}{|\ln R|}\right)Y_B+\frac{cL\alpha}{\lambda N}\exp\left[\frac{\Lambda-z}{\Lambda}\ln(\mathrm{Re}^{-i\delta})\right]\int_z^{z+\lambda}dz'e^{ikz'}\sum_{j=1}^{N}\delta(z'-z_j)\sigma_j.\tag{20f}$$

In spite of the significant increase in formal complexity relative to Eqs. (15), Eqs. (20) are ideally suited for the implementation of the uniform-field limit. This is a situation where one imagines reducing the transmittivity of the mirrors in step with the absorption coefficient of the medium αL, and the cavity mistuning parameter δ, until

$$\alpha L\ll 1,\quad T\ll 1,\quad \delta\ll 1,\tag{21a}$$

in such a way that

$$\frac{\alpha L}{|\ln R|}\approx\frac{\alpha L}{T}\equiv 2C=(\text{finite number}),\tag{21b}$$

$$\frac{\delta}{|\ln R|}\approx\frac{\delta}{T}\equiv\theta=(\text{finite number}).\tag{21c}$$

Physically, a lower absorption coefficient makes the cavity field more uniform longitudinally and, of course, it decreases the influence of the atoms on the field. However, decreasing the transmittivity lengthens the lifetime of the field inside the cavity, and this allows the medium to affect the field in a nontrivial way over a sufficient number of passes. The gradual reduction of the mistuning parameter, as the transmittivity (and hence the modal width) decreases, allows the injected field to remain detuned from the cavity resonance by an amount of the order of the cavity linewidth. The uniform field limit is a well tested approximation in laser physics, and has been shown to hold accurately even for quite realistic values of the parameters αL, T, and δ [13].

In the uniform-field limit the equations describing this model take the much more manageable form

$$\frac{dz_j}{dt}=\frac{p_j}{m},\tag{22a}$$

$$\frac{dp_j}{dt}=-\frac{\hbar k}{4}\gamma_\parallel\sigma_j(Y_F^*e^{-ikz_j}-Y_B^*e^{ikz_j})+\text{c.c.},\tag{22b}$$

$$\frac{d\sigma_j}{dt}=i(\omega-\omega_A)\sigma_j+\gamma_\perp\sigma_{zj}(Y_Fe^{ikz_j}+Y_Be^{-ikz_j})-\gamma_\perp\sigma_j,\tag{22c}$$

$$\frac{d\sigma_{zj}}{dt}=-\frac{\gamma_\parallel}{2}[\sigma_j(Y_F^*e^{-ikz_j}+Y_B^*e^{ikz_j})+\text{c.c.}]-\gamma_\parallel(\sigma_{zj}-\sigma_{zj}^{eq}),\tag{22d}$$

$$\left(\frac{\partial}{\partial t}+c\frac{\partial}{\partial z}\right)Y_F=\kappa Y_I-\kappa(1+i\theta)Y_F+\frac{\kappa 2C\Lambda}{\lambda N}\times\int_z^{z+\lambda}dz'e^{-ikz'}\sum_{j=1}^{N}\delta(z'-z_j)\sigma_j, \tag{22e}$$

$$\left(\frac{\partial}{\partial t}-c\frac{\partial}{\partial z}\right)Y_B=-\kappa(1+i\theta)Y_B+\frac{\kappa 2C\Lambda}{\lambda N}\times\int_z^{z+\lambda}dz'e^{ikz'}\sum_{j=1}^{N}\delta(z'-z_j)\sigma_j, \tag{22f}$$

with the further constraint of the boundary conditions (17).

In arriving at Eqs. (22c) and (22d) for the atomic internal coordinates we have added phenomenological damping terms, as usual; for the case of absorbing atoms, we have $\sigma_{zj}^{eq}=-1$. We note that the field equations (22e) and (22f) are driven and damped in a natural way (i.e., without the need for including phenomenological terms), as a result of our explicit consideration of the resonator boundary conditions.

The momentum equation, instead, is not complete for the purpose of describing the physical problem of interest. In fact, if the center of mass momentum distribution happens to be removed from thermal equilibrium, and if the fields are suddenly turned off, the atomic momenta do not evolve further. What is needed, clearly, is an additional mechanism by which the atoms can regain their thermal equilibrium state in the absence of the driving fields. Because, as already mentioned, most CARL experiments, so far, have been carried out in the presence of a buffer gas at a higher partial pressure than that of the optically active medium, the natural thermalization mechanism in this case is provided by the collisions between the atoms and the buffer gas.

A theoretical framework for the description of the collisional effects in the context of the two-mode model of the CARL (with no cavity) was proposed and analyzed in Ref. [10]. We will summarize in Sec. III some relevant aspects of this approach, as it applies to our theoretical setting, but, first, we proceed to derive the final form of the equations.

We begin by observing that the boundary conditions (17) are consistent with the modal expansions

$$Y_F(z,t)=\sum_{n=-\infty}^{+\infty}f_n(t)e^{i2\pi nz/\Lambda}, \tag{23a}$$

$$Y_B(z,t)=\sum_{n=-\infty}^{+\infty}b_n(t)e^{-i2\pi nz/\Lambda}, \tag{23b}$$

where the modal functions obey the orthonormality relation

$$\frac{1}{\Lambda}\int_0^{\Lambda}dze^{i2\pi mz/\Lambda}e^{-i2\pi nz/\Lambda}=\delta_{n,m}. \tag{24}$$

With the help of Eqs. (23), and on the basis of the uniform-field limit, the only surviving modal amplitudes for the forward and backward fields obey the equations

$$\frac{df}{dt}=\kappa Y_I-\kappa(1+i\theta)f+\frac{\kappa 2C}{\lambda N}\int_0^{\Lambda}dz\int_z^{z+\lambda}dz'e^{-ikz'}\sum_{j=1}^{N}\delta(z'-z_j)\sigma_j, \tag{25a}$$

$$\frac{db}{dt}=-\kappa(1+i\theta)b+\frac{\kappa 2C}{\lambda N}\int_0^{\Lambda}dz\int_z^{z+\lambda}dz'e^{ikz'}\sum_{j=1}^{N}\delta(z'-z_j)\sigma_j, \tag{25b}$$

where we have dropped the subscript "0" from f_0 and b_0. Finally, we can put the right hand sides of Eqs. (25) in a form which is more convenient for the purpose of the numerical calculations with the help of the approximate equality

$$\int_0^{\Lambda}dz\int_z^{z+\lambda}dz'g(z')\approx\lambda\int_0^{L}dz'g(z'), \tag{26}$$

which holds if $\Lambda\gg\lambda$, and if the function $g(z)$ vanishes outside the domain occupied by the medium ($0\leqslant z\leqslant L$). After replacing Eqs. (23) in the atomic equations (22b)–(22d) and retaining only the surviving field modal amplitudes, the final form of our equations is

$$\frac{dz_j}{dt}=\frac{p_j}{m}, \tag{27a}$$

$$\frac{dp_j}{dt}=-\frac{\hbar k}{4}\gamma_{\parallel}\sigma_j(f^*e^{-ikz_j}-b^*e^{ikz_j})+\text{c.c.}, \tag{27b}$$

$$\frac{d\sigma_j}{dt}=-[\gamma_{\perp}-i(\omega-\omega_A)]\sigma_j+\gamma_{\perp}\sigma_{zj}(fe^{ikz_j}+be^{-ikz_j}), \tag{27c}$$

$$\frac{d\sigma_{zj}}{dt}=-\frac{\gamma_{\parallel}}{2}[\sigma_j(f^*e^{-ikz_j}+b^*e^{ikz_j})+\text{c.c.}]-\gamma_{\parallel}(\sigma_{zj}-\sigma_{zj}^{eq}), \tag{27d}$$

$$\frac{df}{dt}=\kappa Y_I-\kappa(1+i\theta)f+\kappa 2C\frac{1}{N}\sum_{j=1}^{N}e^{-ikz_j}\sigma_j, \tag{27e}$$

$$\frac{db}{dt}=-\kappa(1+i\theta)b+\kappa 2C\frac{1}{N}\sum_{j=1}^{N}e^{ikz_j}\sigma_j. \tag{27f}$$

Note that if we ignore the center of mass motion, i.e., if the variables $z_j(t)$ are constant in time, Eqs. (27) in the continuum limit reduce to Eqs. (20) of Ref. [1].

III. A THERMALIZATION MECHANISM FOR THE MOMENTUM DEGREES OF FREEDOM

A major difference between the physics of most CARL laboratory studies and that of the existing models is the absence, in the theories, of a way to account for the effects of the collisions between the optically active atoms and the buffer gas. This deficiency becomes critical when one has to decide if the observed growth of the backward field is induced by the emergence of a density grating, as predicted by the CARL theory, or by a process of the type described in Ref. [1]. The former mechanism has been judged to be unrealistic in steady state, at least at room temperature, while the latter would seem to be possible even in the presence of perturbing collisions [14].

Following the lead of Ref. [10], we introduce collisions between optically active atoms and the buffer gas with the help of a numerical simulation which aims to reflect the main microscopic features of the process. Each optically active atom evolves under the action of the deterministic equations (27). At some randomly selected time, one of these atoms, chosen at random, undergoes an elastic collision, whose effect is to change the momentum of its center of mass and the phase of its polarization. We neglect the rare collisions between pairs of optically active atoms, and collisions involving more than two atoms at a time.

For simplicity, we assume that the colliding partners have the same mass and that the collision is governed by the laws of classical mechanics. Thus, the momentum of the optically active atom, just after collision, matches that of the colliding partner just before collision; the latter, in turn is selected at random from a thermal (Gaussian) distribution. At the same time, the phase of the polarization of this atom jumps to a new value, chosen randomly from a uniform distribution within the interval $[0,2\pi]$. The evolution then proceeds deterministically until the next collision, when another randomly selected atom undergoes the same process described above. This procedure is continued for as long as needed, usually until the average variables have completed the transient phase of their evolution. In the course of these calculations we store, for later processing, time-dependent information on the atomic momenta and positions, the internal degrees of freedom, and the cavity forward and backward fields. The algorithm is briefly sketched in the Appendix.

The random times between collisions are selected in such a way as to conform with the exponential probability density

$$P(t)=\lambda e^{-\lambda t}, \tag{28}$$

where t denotes the time between two consecutive collisions, in units of $1/\gamma_\perp$, and λ is the dimensionless collision rate. Obviously the average time between collisions, $\overline{t_c}$, is given by $1/\lambda$ and this is adjustable in the simulation.

This model assumes that the buffer gas is optically inert, and that its density is much larger than that of the active atoms. Moreover, the buffer gas is supposed to be at thermal equilibrium (in the experiments, this condition is primarily maintained by collisions of the buffer gas atoms with the walls of the cell). On the basis of these assumptions, we conclude that the momentum distribution of the buffer gas is not affected appreciably by the collisions with the active atoms and it always remains Gaussian. The variance of this distribution, σ_P^2, is an adjustable parameter, proportional to the temperature of the buffer gas.

The values of $\overline{t_c}$ selected in our simulations are consistent with the typical experimental pressures. For example, a choice of $\overline{t_c}=30$ corresponds to a pressure of 0.06 mbar, if argon is used as the buffer gas and sodium as the active atoms. However, we have been unable to be uniformly consistent in the selection of the values of σ_P^2 which, in the simulations shown in this paper, are considerably smaller than they should be at room temperature. This selection was motivated by our need for using the homogeneously broadened results of Ref. [1] as a guide in our search for nontrivial solutions. A major advantage of that model is that a linear stability analysis makes it possible to predict in advance for which combination of parameters interesting effects are likely to emerge. This strategy is not available with the present microscopic model, and a search for nontrivial solutions under room temperature conditions calls for the analysis of a very large parameter space and a very substantial computational effort which we may undertake in future work. The study of a mildly inhomogeneous system and the guidance offered by the solutions of Ref. [1] reduced the guesswork required by the identification of appropriate parameters.

We should mention also that our model becomes realistic only in the limit when the number of atoms is sufficiently large. Thus, we have made special efforts to carry out each numerical simulation for several system sizes, until we found convincing evidence that no quantitative changes in the predicted results would emerge from a further increase in the number of atoms. As a compromise, we have attempted to meet these requirements by selecting sufficiently small values for the width of the momentum distribution even though this implies much lower temperatures than used in the experiments.

IV. DISCUSSION OF THE RESULTS AND COMPARISON WITH OTHER MODELS

As we have already mentioned, the model developed in this paper is closely related to the one discussed in Ref. [1], but it also includes the effects of recoil, as required in the context of the theory of the CARL, and collisions with a buffer gas, which are not included in [1] and [5]. The latter feature is necessary not only because a buffer gas was often used in the experiments, but also because it provides the natural mechanism for the emergence of a steady state, in the presence of the driving field, and for the eventual return of the atoms to thermal equilibrium, if the driving field is turned off at some point. Collisions and recoil introduce Doppler and pressure broadening in the model, and this marks another difference relative to the settings of Refs. [1] and [5]

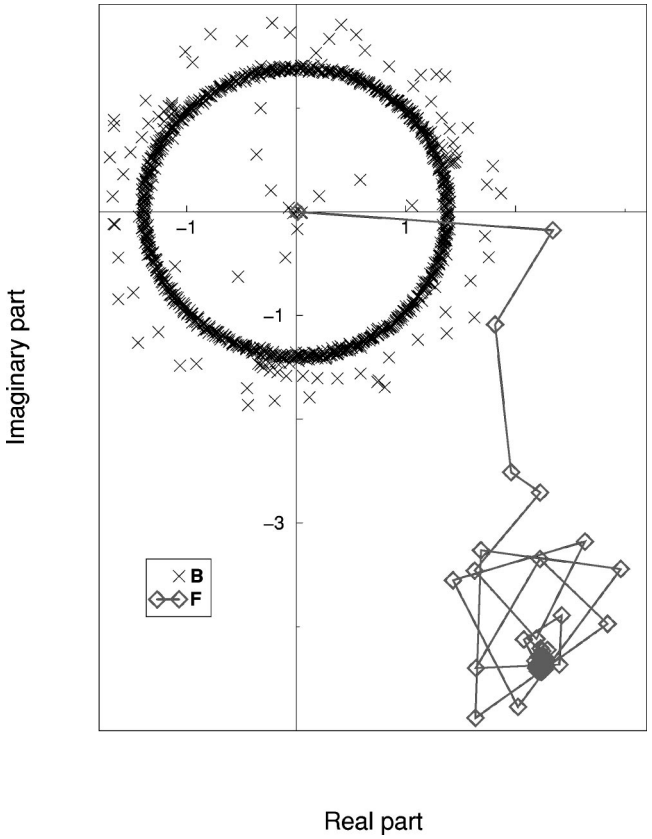

FIG. 2. The imaginary parts of *f* and *b* are plotted as functions of their respective real parts. The forward and backward fields are represented, respectively, by diamonds (*F*) and crosses (*B*). Initially, both fields are nearly zero and evolve into a nonsynchronous steady state. The parameters are $Y_I=45$, $\tilde{\delta}_A=-0.1$, $C=39.5$, $\tilde{\kappa}=0.55$, $\theta=9$, $\sigma_P=10$, $\tilde{\gamma}=2$, $\tilde{\Omega}_r=2.07\times10^{-2}$, $\overline{t_c}=30.3$. The value chosen for $\tilde{\Omega}_r$ corresponds to the D_2 line of sodium.

which dealt, instead, with homogeneously broadened systems.

We recall that Ref. [1] predicts the emergence of a number of solutions which include the following.

(i) ''Trivial'' solutions matching the well known behavior of a bistable system in a unidirectional resonator. These solutions correspond to a stationary nonzero forward field and zero backward field.

(ii) ''Self-pulsing'' solutions, where both forward and backward field intensities oscillate in time, and others where the backward field is absent altogether.

(iii) ''Nonsynchronous'' solutions, where both forward and backward field intensities are time independent, the forward field oscillates with the frequency of the injected signal, and the backward field is frequency shifted, apparently as a result of a frequency pulling effect. The term ''nonsynchronous'' is meant to emphasize that the coexisting cavity fields do not share the same carrier frequency.

In the model described in this paper, we found the same type of long time solutions, except for the one where *both* backward and forward fields are self-pulsing.

An example of a nonsynchronous solution is shown in Fig. 2 where we plot the imaginary parts of both forward and backward fields as functions of the respective real parts, while the fields evolve in time. Starting from very small initial values of the real and imaginary parts, the forward field evolves into a configuration corresponding to the cluster of open diamonds labeled by *F*. Because the reference frequency selected in our calculations is the carrier frequency of the external driving field, the time-independent character of the long-time forward field indicates that this field is locked to the external signal. The real and imaginary parts of the backward field, instead, oscillate harmonically at a constant rate. This implies that the backward field has a different carrier frequency from that of the injected signal. In this case, the frequency shift between backward and forward fields is $\omega_b-\omega_f=-4.16$, in normalized units of $\gamma_\perp$. Depending on the parameters, we have observed positive or negative detuning values, as one would expect if the frequency shift experienced by the backward field was a consequence of a standard mode-pulling effect [15]. The behavior of this nonsynchronous solution is qualitatively identical to the one discussed in Ref. [1].

By contrast, an example of a self-pulsing solution with zero backward field is shown in Fig. 3, also with the help of a complex plane portrait of the fields. The parameters are such that the backward field, after a small initial growth, loses its competition with the forward field and decays essentially to zero, apart from fluctuations introduced by the stochastic features of the simulation (cluster of crosses labeled *B*); the real and imaginary parts of the forward field vary roughly harmonically in time, and the intensity undergoes simple self-pulsing oscillations, as shown in Fig. 4.

In the presence of counterpropagating waves with slightly different carrier frequencies, one expects the total field to acquire a traveling modulated intensity pattern whose imprint should appear in the spatial distribution of the population difference. This is clearly seen from the nonsynchronous solution shown in Fig. 5, where the population difference of each atom (the probability of being in the excited state minus the probability of being in the ground state) is plotted as a function of its normalized position. A surprising feature of these results is the appearance of a substantial fraction of atoms in an inverted state, as already noted (see Fig. 7 of Ref. [1]). Unfortunately, we are still unable to offer a plausible physical interpretation of this interesting effect, except to say that it could be evidence of underlying atomic coherence. This grating of population is actually a traveling structure, as slightly delayed patterns clearly show.

A companion traveling wave develops also for the modulus of the atomic polarization variable, and this is illustrated in Fig. 6 for the same parameters used in Fig. 5. The real and imaginary parts of the atomic polarization, instead, give intricate structures which we have been unable to interpret and whose shapes change in a complex way as a function of time. For the sake of illustration, a plot of the polarization in the complex plane shows a ''dumbbell'' structure that rotates around the center of symmetry, preserving its shape as time evolves (Fig. 7 shows this structure for a specific value of time).

A special aim of our simulations was to clarify the role played by the atomic density grating in promoting the growth

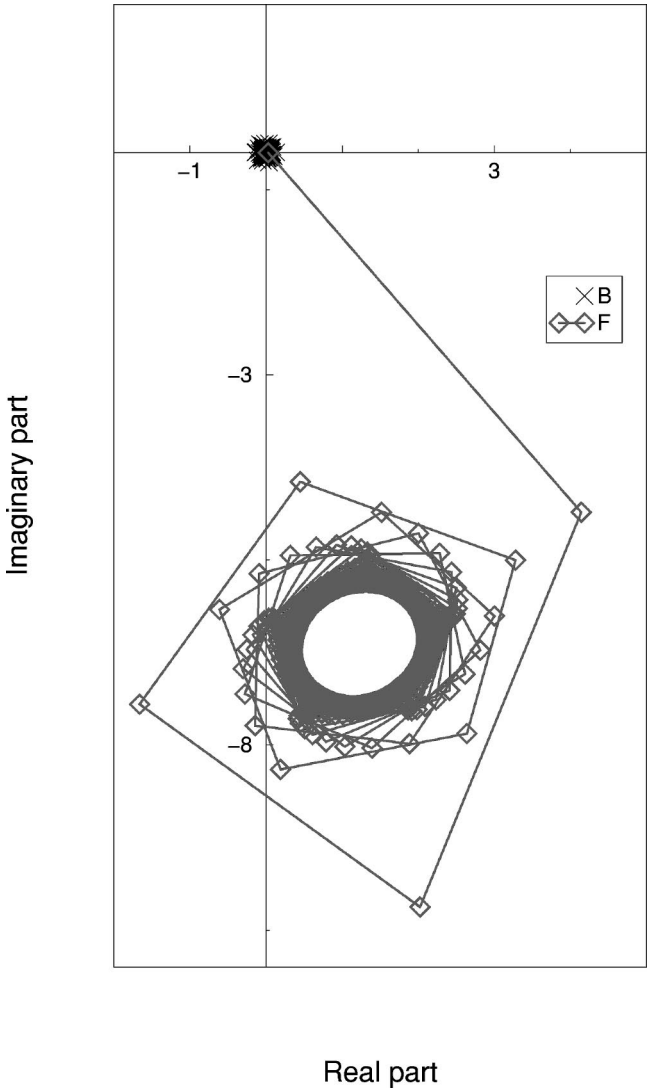

FIG. 3. The imaginary parts of f and b are plotted as functions of their respective real parts. The forward and backward fields are represented, respectively, by diamonds (F) and crosses (B). Initially, both fields are nearly zero and evolve into a self-pulsing state. The parameters are $Y_I=100$, $\tilde{\delta}_A=-0.1$, $C=39.5$, $\tilde{\kappa}=0.55$, $\theta=15$, $\sigma_P=10$, $\tilde{\gamma}=2$, $\tilde{\Omega}_r=2.07\times10^{-2}$, $\overline{t_c}=30.3$.

of the backward field and, eventually, in supporting a stable nontrivial steady state. For this purpose, we monitored the evolution of the bunching parameter defined in Ref. [5] as

$$b=\left|\frac{1}{N}\sum_{j=1}^{N}e^{ikz_j}\right|. \tag{29}$$

Obviously, if the optically active atoms are uniformly distributed, b must be equal to zero, and its growth gives an indication that the atomic density function has acquired a spatial structure. Indeed, the bunching parameter grows during the early stage of the evolution, regardless of the subsequent behavior of the system, but then it decays and becomes negligibly small for long times, even in the presence of a well developed backward field.

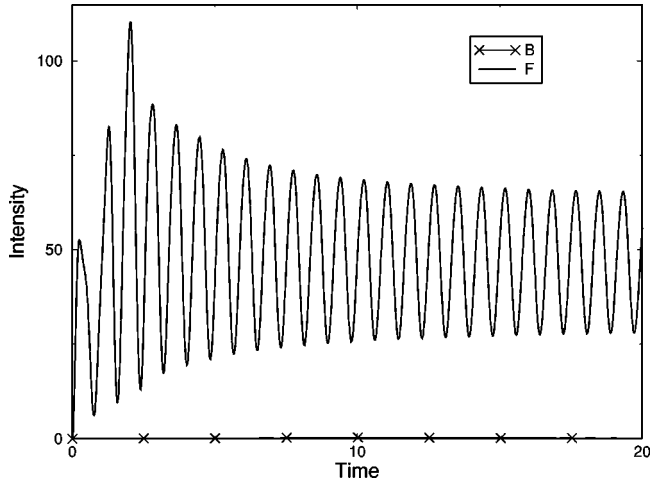

FIG. 4. The intensities of both fields, $|f|^2$ and $|b|^2$, labeled, respectively, F and B, are plotted as functions of time. The parameters are identical to those of Fig. 3. Note that the stationary intensity of the backward field is zero.

The decay time of the bunching parameter (an example is shown in Fig. 8) is of the order of the average time between collisions, $\overline{t_c}$, and this suggests that ordered spatial structures are, at best, only transient phenomena which eventually disappear as a result of the collisions between the optically active atoms and the buffer gas. This feature was noted in a number of simulations discussed in Ref. [10], and was also considered by others as a transient phenomenon [9]. We searched for the possible existence of a density grating under steady state conditions by direct analysis of the spatial distribution of the atomic center of mass coordinates, but we found no evidence for it. However, we did observe a clear spatial structure at the time when the bunching parameter b reached its maximum value, as shown in Fig. 9.

We take this as evidence that this fragile structure may not be able to survive, except perhaps at much lower tempera-

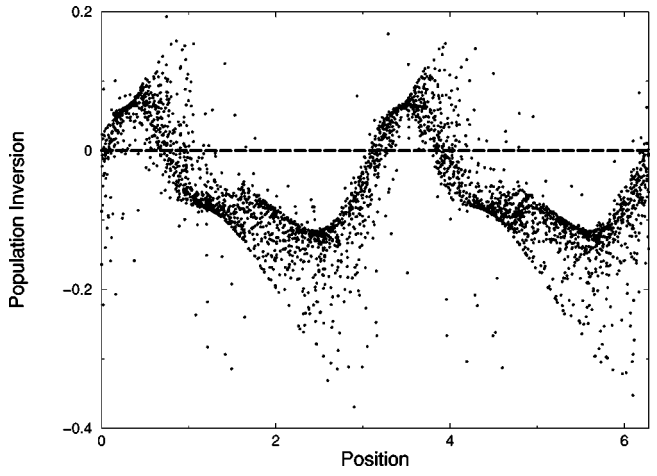

FIG. 5. The population inversion of each atom is plotted as a function of its position. This is done at a given time, after the fields have reached a nonsynchronous state. The thick dashed line represents the boundary that separates groups of excited and unexcited atomic states. The parameters are identical to those of Fig. 2.

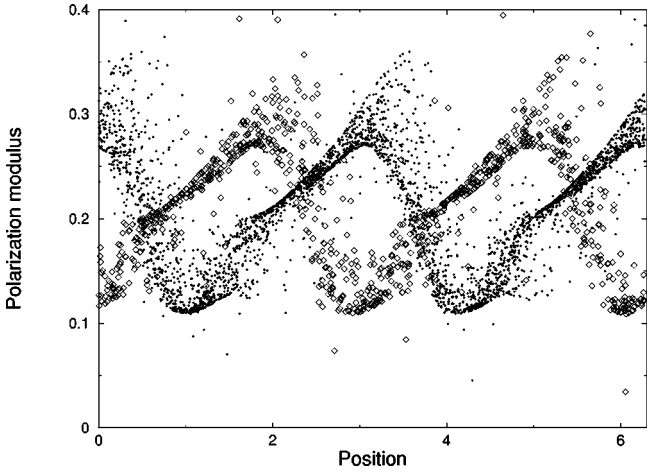

FIG. 6. The modulus of the polarization of each atom is plotted as a function of its position after all transients have died off. At a given time t_0 the data are plotted with open diamonds, while at the time $t_0+0.5$ they are plotted with solid dots. The parameters are identical to those of Fig. 2.

tures, where, conceivably, our semiclassical description may no longer be applicable. Thus, on the basis of our findings, the mechanism of growth of the backward field appears to stem mainly from the emergence of the polarization grating, as already suggested in Ref. [7] on the basis of theoretical and experimental considerations.

The model adopted in this work for the simulation of collisions is conceptually direct but is also computationally very intensive. Earlier studies of the CARL [9] advanced an appealing alternative scheme. In our notations, this amounts to adding to Eq. (27b) a phenomenological damping term of the form

$$\left(\frac{dp_j}{dt}\right)_{coll} = -\gamma_c(p_j - p_j^{eq}), \tag{30}$$

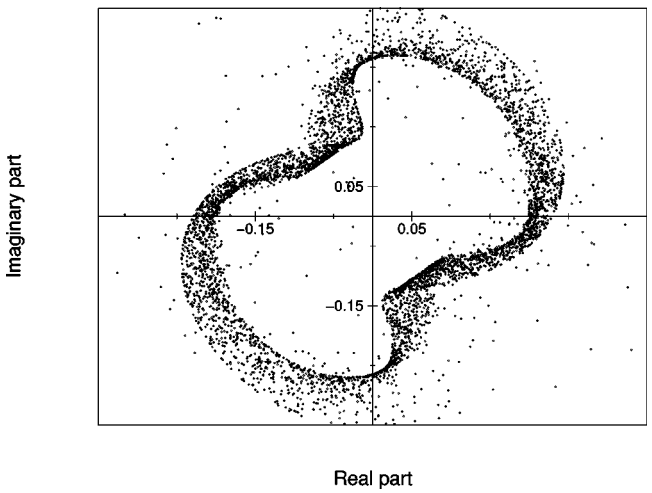

FIG. 7. The imaginary part of the polarization of each atom is plotted as a function of the corresponding real part after reaching a nonsynchronous state. The parameters are identical to those of Fig. 2.

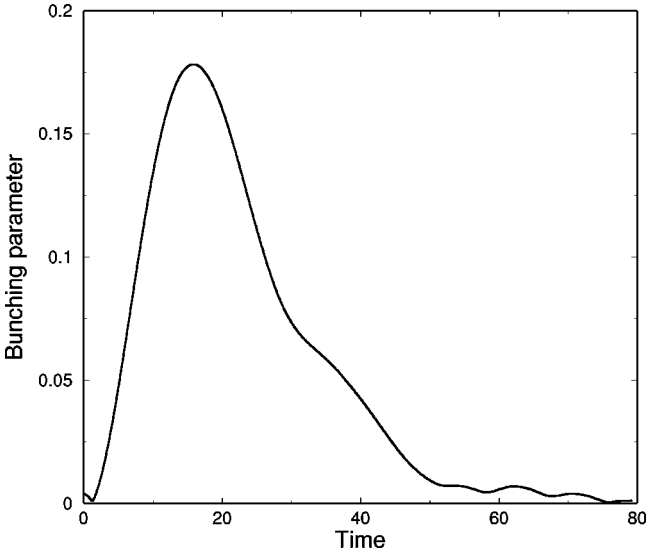

FIG. 8. The bunching parameter is plotted as a function of time at the beginning of the evolution. The parameters are identical to those of Fig. 2.

where γ_c is the thermalization rate due to collisions and p_j^{eq} is the thermal equilibrium value of the momentum of the jth atom. At the start of the simulation, according to this scheme, one selects a collection of random values of p_j, having a Gaussian distribution with a chosen width, and then allows the atomic and field variables to evolve deterministically according to the time-dependent equations of motion (27). Each atom, during the evolution, would continue to be associated with the initial selection of its equilibrium momentum, p_j^{eq}. This model, to which we refer informally as the phenomenological momentum damping (PMD) model, has the obvious virtue that, if one should turn off the interaction of the atoms with the cavity field(s), the atomic ensemble

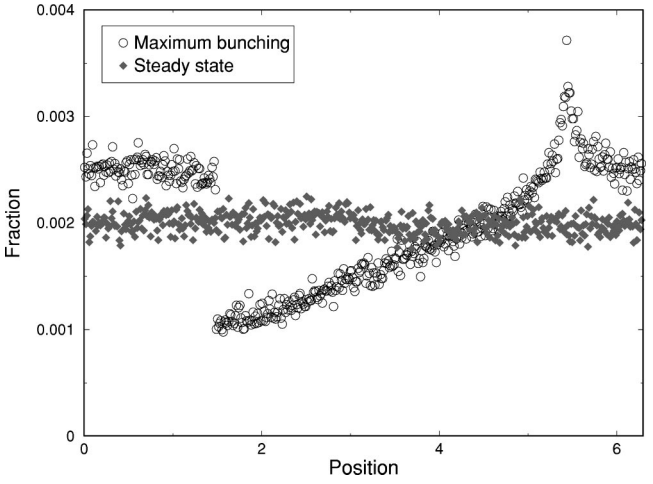

FIG. 9. A histogram of the atomic density in the cell is plotted as a function of position for two different times: the open circles correspond to the time when the bunching parameter, shown in Fig. 8, acquires a maximum value; the solid diamonds correspond to the solution after all transients have died off. The parameters are identical to those of Fig. 2.

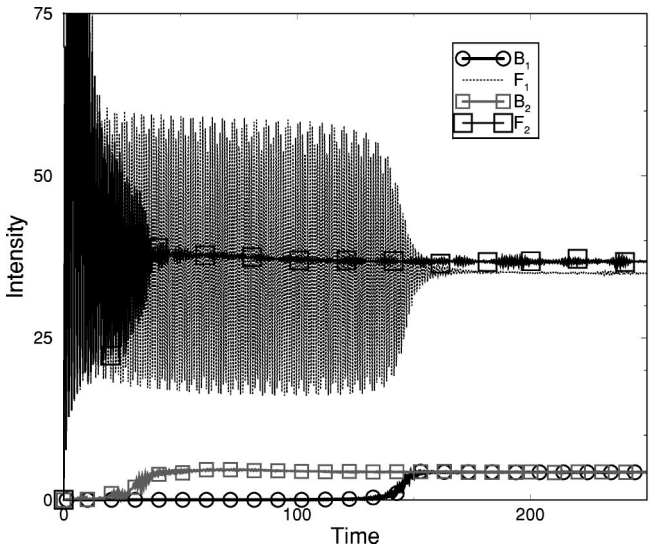

FIG. 10. The intensities of both fields, $|f|^2$ and $|b|^2$, labeled, respectively, *F* and *B*, are plotted as functions of time. The results of the PMD model are indexed with the subscript ''1''; those of the microscopic model are indexed by ''2.'' The parameters of these simulations are $Y_I=90$, $\tilde{\delta}_A=2$, $C=50$, $\tilde{\kappa}=0.5$, $\theta=-10$, $\sigma_P=10$, $\tilde{\gamma}=2$, $\tilde{\Omega}_r=2.07\times10^{-2}$, $\overline{t_c}=30.3$, for the microscopic model, and $\gamma_c=1/30.3$ for the PMD model.

would relax to thermal equilibrium, by construction, in a time of the order of $1/\gamma_c$. We also note that the polarization relaxation process is not directly affected by the momentum relaxation, although $\gamma_\perp$ can be modified by hand to account for the presence of collisions (i.e., it can be made larger than its radiative limit to simulate collisional broadening effects).

Nevertheless, it is not clear if this approach is satisfactory, nor if it has much in common with the microscopic description developed in Ref. [10] and adopted in this work. We have looked into this matter and compared the results of our microscopic simulations against those obtained by integrating Eqs. (27) after inclusion of the phenomenological damping terms given by Eq. (30). We have carried out this comparison by using the same parameters, and by selecting $\gamma_c=1/\overline{t_c}$. Our results are inconclusive, but we feel that they deserve to be reported in order to provide some guidance for possible future studies.

Both the microscopic and the PMD models evolve into ''plausible'' long time solutions, i.e., they show no evidence for the type of evolution displayed by the early simulations of Ref. [5]. However, we have been unable to identify sets of parameters for which we could find clear agreement or disagreement. In some instances, typically for low collision rates, we have seen evidence of reasonable quantitative agreement between the stationary intensities of nonsynchronous solutions (but not for their transient values). An example is shown in Fig. 10.

The corresponding stationary momentum distributions, instead, are very different from one another: the distribution associated with the PMD model is Gaussian even in the presence of forward and backward fields, and its width coincides with the selected initial value, while the one resulting from

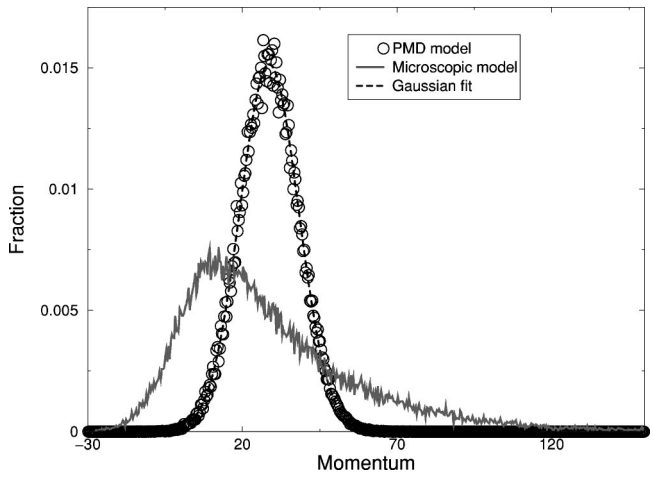

FIG. 11. The momentum distributions corresponding to the PMD model (open circles) and to the microscopic model (solid line). The dashed line represents a fit to a Gaussian distribution of width $\sigma_{fit}=9.47$. The parameters are identical to those of Fig. 10.

the microscopic model is very significantly nonthermal, as shown in Fig. 11. Intuitively, a nonthermal distribution would appear to be the more plausible of the two results.

After increasing the collision rate by a factor of 100, the two models yield identical momentum distributions having a Gaussian profile (see Fig. 12). However, the corresponding steady state intensities are entirely different from each other: the microscopic model leads to a nonsynchronous steady state, while the PMD calculation produces a trivial solution with zero backward field, as shown in Fig. 13.

In aggregate, the solutions displayed in Figs. 11 and 12 suggest that, at least for the chosen parameters, the PMD model is unable to describe possible departures from a state of thermal equilibrium. It is tempting to speculate that an important source of disagreement between the two models is the ''noise'' introduced by the microscopic simulation of the

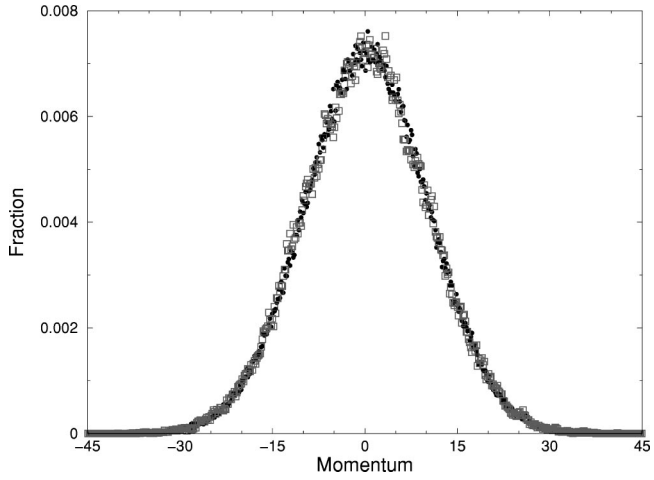

FIG. 12. The momentum distributions corresponding to the PMD model (open squares) and to the microscopic model (solid dots). The parameters of these simulations are $Y_I=90$, $\tilde{\delta}_A=2$, $C=50$, $\tilde{\kappa}=0.5$, $\theta=-10$, $\sigma_P=10$, $\tilde{\gamma}=2$, $\tilde{\Omega}_r=2.07\times10^{-2}$, $\overline{t_c}=0.3$ for the microscopic model, and $\gamma_c=1/0.3$ for the PMD model.

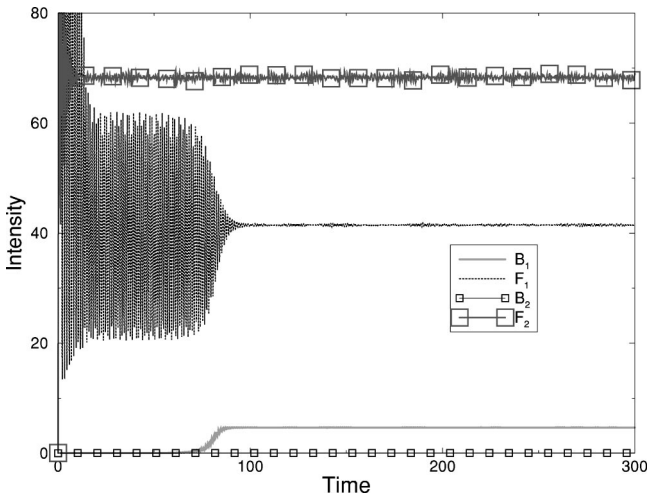

FIG. 13. The same as Fig. 10 with a 100-fold increase in the collision rate. The parameters are identical to those of Fig. 12.

collisions. For different combinations of parameters both models display different kinds of solutions. As the parameters are varied in a fully deterministic model, one type of long time solution gives way to a different one, beyond its stability boundary. In the presence of noise, transitions between one domain and another, especially if the domains coexist, can easily occur ''spontaneously.'' In the absence of a detailed stability map of the various solutions, there seems to be no easy way to resolve this interesting issue.

V. SUMMARY AND CONCLUSIONS

In this paper we have developed a microscopic description of the collective atomic recoil laser in an optical resonator. This work complements and generalizes earlier studies of bidirectional optical bistability [1] and of the CARL [5] with the inclusion of the effects of collisions between the optically active atoms and a buffer gas. The purpose of this added feature is twofold: it allows the average dynamical variables to approach physically reasonable long time behaviors (steady state or self-pulsing), and it simulates an important aspect of the experimental settings.

Our main predictions include the existence of a class of stationary solutions (nonsynchronous steady states) in which the ring resonator can support both forward and backward fields oscillating with different carrier frequencies. The growth of the backward field in the early stage of the evolution is accompanied by the appearance of a transient structure in the atomic density profile which then disappears in a time of the order of the average time between collisions. In the presence of forward and backward cavity fields, the optically active atoms acquire a spatial modulation of the polarization and population difference which, unlike the early density modulation, persists for arbitrarily long times. Furthermore, the momentum distribution, which we assume to be Gaussian at the beginning of the evolution displays significant departures from the state of thermal equilibrium and remains in this nonequilibrium configuration for as long as the cavity fields are kept different from zero.

We have carried out a comparison between the results of our microscopic model and an earlier proposal advanced by Bonifacio and Verkerk [9]. The results do not match, but it is probably too early to draw negative conclusions. In addition, this earlier proposal is appealing and less computationally intensive than ours. We feel that additional investigations are warranted.

ACKNOWLEDGMENTS

We are most grateful to Jorge Tredicce, Gian Luca Lippi, Antonio Politi, and Julien Javaloyes for extensive discussions and useful advice throughout the development of this research.

APPENDIX

This appendix outlines the approach used in this paper for the numerical solution of the equations of motion, including the microscopic simulation of the collisions. As the starting point, we consider a rescaled version of Eqs. (27), after introducing the dimensionless variables

$$\tilde{p}_j=\frac{p_j}{\hbar k},\quad \tilde{z}_j=kz_j,\quad \tau=\gamma_\perp t, \tag{A1}$$

and the scaled parameters

$$\tilde{\kappa}=\frac{\kappa}{\gamma_\perp},\quad \tilde{\gamma}=\frac{\gamma_\parallel}{\gamma_\perp},\quad \tilde{\Omega}_r=\frac{\omega_r}{\gamma_\perp},\quad \tilde{\delta}_A=\frac{\omega_A-\omega}{\gamma_\perp}, \tag{A2}$$

where $\omega_r\equiv 2\hbar k^2/m$ is the frequency shift associated with the single-photon recoil. In terms of the new variables and parameters, Eqs. (27) take the form

$$\frac{d\tilde{z}_j}{d\tau}=\frac{1}{2}\tilde{\Omega}_r\tilde{p}_j, \tag{A3a}$$

$$\frac{d\tilde{p}_j}{d\tau}=-\frac{1}{4}\tilde{\gamma}\sigma_j(f^*e^{-i\tilde{z}_j}-b^*e^{i\tilde{z}_j})+\text{c.c.}, \tag{A3b}$$

$$\frac{d\sigma_j}{d\tau}=-(1+i\tilde{\delta}_A)\sigma_j+\sigma_{zj}(fe^{i\tilde{z}_j}+be^{-i\tilde{z}_j}), \tag{A3c}$$

$$\frac{d\sigma_{zj}}{d\tau}=-\frac{1}{2}\tilde{\gamma}[\sigma_j(f^*e^{-i\tilde{z}_j}+b^*e^{i\tilde{z}_j})+\text{c.c.}]-\tilde{\gamma}(\sigma_{zj}-\sigma_{zj}^{eq}), \tag{A3d}$$

$$\frac{df}{d\tau}=\tilde{\kappa}Y_I-\tilde{\kappa}(1+i\theta)f+\tilde{\kappa}2C\frac{1}{N}\sum_{j=1}^{N}e^{-i\tilde{z}_j}\sigma_j, \tag{A3e}$$

$$\frac{db}{d\tau}=-\tilde{\kappa}(1+i\theta)b+\tilde{\kappa}2C\frac{1}{N}\sum_{j=1}^{N}e^{i\tilde{z}_j}\sigma_j, \tag{A3f}$$

where the range of variation of the scaled position variable $\tilde{z}_j$ is the interval $[0;2\pi]$. The initial conditions correspond to a state of thermal equilibrium for the optically active atoms

(i.e., the spatial distribution is uniform, while the momentum distribution is Gaussian). The cavity fields are initially chosen to be very small, for the purpose of modeling the influence of spontaneous emission (typical values are such that the initial real and imaginary parts of both fields are set equal to 10^{-10}). We have verified that the chosen initial conditions have no influence on the long time solutions, but only on the details of the transient regimes. This is, typically, to be expected especially in the presence of the randomizing effects introduced by the collisions.

Now, we briefly consider the implementation of the collision algorithm already introduced in Sec. III. The main steps can be described as follows.

(a) We initialize the atomic variables, as described above. For N atoms, this requires the selection of $5N+4$ real initial values.

(b) For each atom we pick the random time interval between the beginning of the evolution and the first collision according to the exponential distribution, Eq. (28).

(c) We integrate numerically the deterministic Eqs. (A3) from $\tau=0$ until the occurrence of the very first collision. For this purpose, we start by selecting a nominal integration step, consistent with the required level of accuracy. After selection of the time of occurrence of the first collision, we redefine the integration step, actually used in the calculation, in such a way that the duration of the deterministic evolution is an exact multiple of the integration step which, in turn, we constrain to remain smaller than or equal to the chosen nominal value. In this way, we ensure the accuracy of the numerical integration process and, at the same time, we guard against the possibility that the time of the first collision (or, later in the evolution, the time between consecutive collisions) may turn out to be smaller than the selected integration step.

(d) We modify the momentum and the phase of the polarization of the atom that has just undergone a collision.

(e) We select a new collision time for this atom, while keeping the previously selected collision times of the other atoms in the sample.

(f) We save the relevant values of the variables for future analysis.

(g) We go back to step (c).

Note that this procedure does not involve the initial selection of all the collision times for all the atoms which would require far too much computer memory.

[1] Z. Ye and L. M. Narducci, Phys. Rev. A **63**, 043815 (2001).

[2] See, for example, L. A. Lugiato, in *Progress in Optics*, edited by E. Wolf (Elsevier, Amsterdam, 1984), Vol. XXI, p. 69.

[3] M. L. Asquini and F. Casagrande, Z. Phys. B: Condens. Matter **44**, 233 (1981).

[4] As in [1], ''forward'' denotes the direction of the injected field.

[5] R. Bonifacio and L. De Salvo, Nucl. Instrum. Methods Phys. Res. A **341**, 360 (1994); R. Bonifacio, L. De Salvo, L. M. Narducci, and E. J. D'Angelo, Phys. Rev. A **50**, 1716 (1994).

[6] G. L. Lippi, G. P. Barozzi, S. Barbay, and J. R. Tredicce, Phys. Rev. Lett. **76**, 2452 (1996); P. R. Hemmer, N. P. Bigelow, D. P. Katz, M. S. Shahriar, L. De Salvo, and R. Bonifacio, *ibid.* **77**, 1468 (1996).

[7] W. J. Brown, J. R. Gardner, D. J. Gauthier, and R. Vilaseca, Phys. Rev. A **55**, R1601 (1997); **56**, 3255 (1997).

[8] An early step in this direction, but along more phenomenological lines, was taken by R. Bonifacio, G. R. M. Robb, and B. W. J. McNeil, Phys. Rev. A **56**, 912 (1997).

[9] R. Bonifacio and P. Verkerk, Opt. Commun. **124**, 469 (1996).

[10] M. Perrin, G. L. Lippi, and A. Politi, Phys. Rev. Lett. **86**, 4520 (2001); J. Mod. Opt. **49**, 419 (2002).

[11] L. A. Lugiato and L. M. Narducci, Z. Phys. B: Condens. Matter **71**, 129 (1988).

[12] R. Bonifacio and L. A. Lugiato, Lett. Nuovo Cimento Soc. Ital. Fis. **21**, 505 (1978); **21**, 510 (1978).

[13] L. A. Lugiato, L. M. Narducci, E. V. Eschenazi, D. K. Bandy, and N. B. Abraham, Phys. Rev. A **32**, 1563 (1985).

[14] We make this point because the growth of the backward field in the bidirectional model of Ref. [1] originates from a dynamical instability, and is prompted by background noise. Hence, collisions are, in fact, helpful as the trigger of unstable behavior.

[15] In steady state, the point $(\mathrm{Re}(b),\mathrm{Im}(b))$ traces a circle with an angular frequency equal to the frequency shift. If, as time progresses, the rotation of the point is in the clockwise direction, then the frequency shift of b relative to f is positive; otherwise it is negative.